Evaluation of peristaltic micromixers for highly integrated microfluidic systems

Duckjong Kim, Hoon Suk Rho, Sachin Jambovane, Soojeong Shin, and Jong Wook Hong

---

Articles you may be interested in

Evaluation of peristaltic micromixers for highly integrated microfluidic systems

Duckjong Kim,[1,2] Hoon Suk Rho,[1,3] Sachin Jambovane,[1,4] Soojeong Shin,[5] and Jong Wook Hong[1,5,6,a]

[1]*Materials Research and Education Center, Department of Mechanical Engineering, Auburn University, Auburn, Alabama 36849, USA*
[2]*Department of Nano Mechanics, Korea Institute of Machinery and Materials, Daejeon 34103, South Korea*
[3]*Mesoscale Chemical Systems Group, MESA+ Institute for Nanotechnology, University of Twente, 7500 AE Enschede, The Netherlands*
[4]*Environmental Molecular Sciences Laboratory, Pacific Northwest National Laboratories, Richland, Washington 99352, USA*
[5]*Department of Bionano Engineering, Hanyang University, Ansan 15588, South Korea*
[6]*Department of Bionano Technology, Graduate School, Hanyang University, Seoul 04763, South Korea*

Microfluidic devices based on the multilayer soft lithography allow accurate manipulation of liquids, handling reagents at the sub-nanoliter level, and performing multiple reactions in parallel processors by adapting micromixers. Here, we have experimentally evaluated and compared several designs of micromixers and operating conditions to find design guidelines for the micromixers. We tested circular, triangular, and rectangular mixing loops and measured mixing performance according to the position and the width of the valves that drive nanoliters of fluids in the micrometer scale mixing loop. We found that the rectangular mixer is best for the applications of highly integrated microfluidic platforms in terms of the mixing performance and the space utilization. This study provides an improved understanding of the flow behaviors inside micromixers and design guidelines for micromixers that are critical to build higher order fluidic systems for the complicated parallel bio/chemical processes on a chip. © 2016 AIP Publishing LLC. [http://dx.doi.org/10.1063/1.4940927]

I. INTRODUCTION

In the last decades, to explore the potential of microfluidics, various approaches have been proposed and demonstrated.[1–6] Microfluidic components including valves, pumps, and mixers within polymeric chain reaction (PCR) chips were summarized by Zhang *et al.*,[4] and various liquid handling systems in microfluidic devices to process chemical reactions were reviewed by Livak-Dahl *et al.*[5] Nge *et al.* summarized the history of developing in microfluidic platforms in terms of materials, functionalities, integration, and applications.[6] Among them, the mechanical microfluidic system based on the multilayer soft lithography is recognized as one of the most promising microfluidic platforms.[7,8] When a flow channel passes above a control channel, the thin membrane between the two channels functions as a valve as shown in Fig. 1(a). By increasing the pressure in the control channel, the membrane is deflected and blocks the flow channel. By releasing the pressure, the membrane is restored to its original shape and the flow channel is re-opened.[9,10] Various microfluidic components have been implemented by the sequential control of the valves, and they can be easily integrated into a single chip.[7,11,12] It was demonstrated that plural adjoining valves can function as a peristaltic pump.[7,11–13] Typically, three valves were placed in a series and the air pressure for each valve was increased and released sequentially as shown in Fig. 1(b).

Consequently, the sequential motion of the valves generated fluid flow in the flow channel. When this peristaltic pump operates in a loop, an active micromixer is created.[11] For the peristaltic micromixers, multiple spots of one side of a ring-shaped microchannel are deflected sequentially by using a pneumatic control. This peristaltic motion generates fluid flow in the curved microchannel and, in the course of the flow, the interface between the fluids is stretched very quickly, which improves the mixing significantly. In addition, the mixer can hold the mixed reagents during analysis of the reaction. Due to the incubation capability, the reaction time can be flexibly controlled, and sample waste can be minimized.

The peristaltic micromixers have been used for various applications in the fields of biology and chemistry. Chou *et al.* showed that the mixing of reagents can be efficiently accomplished for molecules possessing different diffusion constants.[11] They also demonstrated that the reaction kinetics of a surface-binding assay can be enhanced by nearly two orders of magnitude. Hong *et al.* demonstrated complicated multiple processes on a chip by using the mixer.[12] They mixed bacterial cells, lysis buffer, and dilution buffer, by using a micromixer and successfully recovered nucleic acids from several bacterial cells. In our previous work, Jambovane *et al.* showed parallel enzymatic reactions for obtaining the kinetic parameters of enzyme reactions. We performed multiple reactions with a concentration gradient of reagents by adapting 11 parallel reactors.[14] An integrated microfluidic device with a bead-based chemosensor was demonstrated by Lee *et al.*[15] They showed protein kinase assays and fluorometric detection

---

a)Author to whom correspondence should be addressed. Electronic mail: jwh@hanyang.ac.kr.
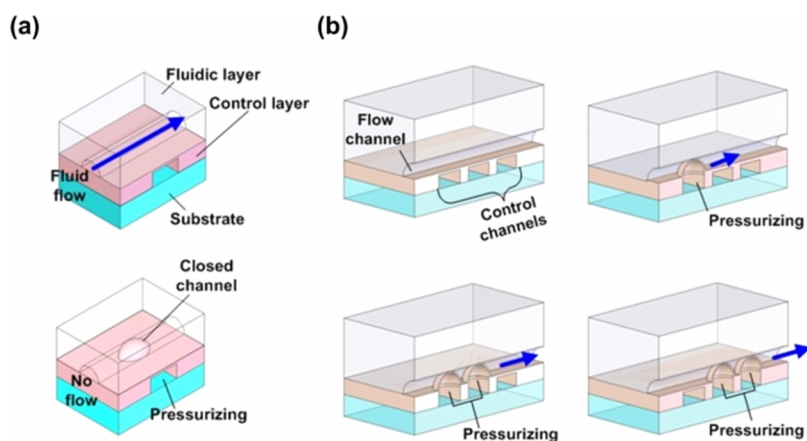
FIG. 1. Schematic diagrams of pneumatically controlled microfluidic devices. (a) Simple on-off valve and (b) peristaltic micro pump (not to scale).

of peptides by integrating a micromixer and a chemosensor. For the chemical applications of a micromixer, Wang *et al.* utilized integrated microfluidics for parallel screening of an *in situ* click chemistry library.[16] Also, a microcontinuous stirred tank reactor was presented by Galas *et al.* for the systematic studies of non-equilibrium chemical processes.[17]

Even though many researchers have reported the versatility of the peristaltic micromixer and have been making efforts to incorporate the mixer into highly integrated microfluidic platforms, the basic design is usually that of the circular mixing loop. For the same length, the circular-shaped mixer requires the largest footprint among the three types of the mixers: circular, rectangular, and triangular. Until now, the geometry has not been optimized for high mixing performance. Since reagent mixing is one of the most time-consuming processes for bio/chemical applications on a chip, maximization of the mixing performance of the mixer is crucial for the successful development of highly integrated microfluidic platforms.

In this study, we investigated the effects of geometry on the mixing performance of the peristaltic micromixer. For the parametric study, we designed and fabricated ten different mixers, varying the distance between the mixing valves, the width of the mixing valve, and the shape of the mixing loop. The membrane thickness was about 20 μm. By using a stereomicroscope and two different colors of dye solutions,

we visualized and captured the mixing phenomena in each mixer, and quantified the mixing performance by analyzing the captured images. Finally, we derived design guidelines for the peristaltic micromixer in highly integrated microfluidic platforms that can be used for complicated parallel reactions on a chip.

II. EXPERIMENTAL

Fig. 2 shows the layout of the mixer chips. Each mixer chip has three different mixers comprised of two layers: the top fluidic layer and the bottom control layer as shown in Fig. 1(a). The fluidic layer has flow channels (blue lines) and the control layer has control channels (yellow and red lines) connected to the shutoff valves and mixing valves. Each mixer has eight shutoff valves as shown in Fig. 2. Among them, two centerline valves initially close two points of the mixing loop to prevent contact between the two fluids to be mixed and are opened when the mixing is started. The other six shutoff valves are initially opened while the two fluids are infused into the mixing loop and are closed during mixing to prevent leakage from the mixing loop. There are three mixing valves in each mixer. By the sequential motion of the valves shown in Fig. 1(b), fluids in the mixing loop are moved and mixed. To investigate the effects of the geometry
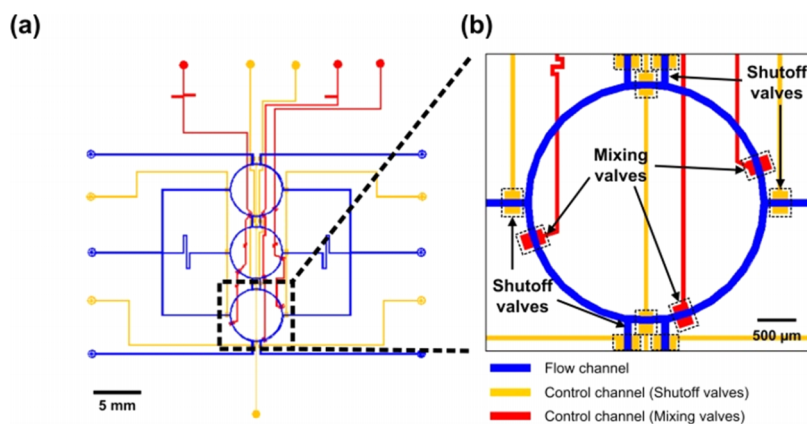

FIG. 2. Layout of the mixer chip (chip B); blue lines, yellow lines, and red lines represent the flow channels, the control channels connected to shutoff valves, and the control channels connected to mixing valves, respectively.
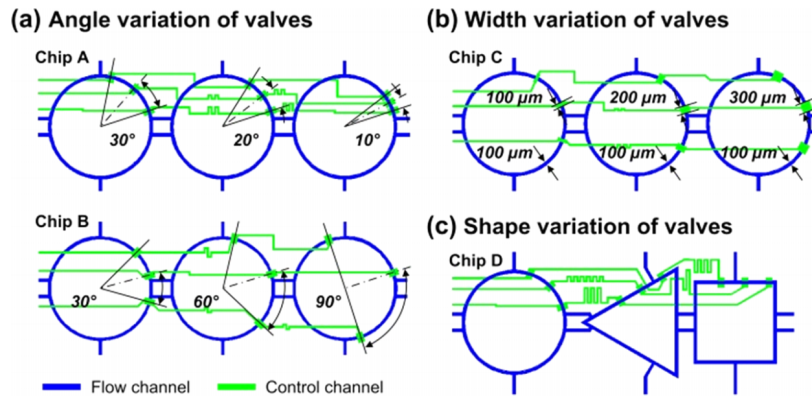
FIG. 3. Mixer chip designs. (a) Angle variation of mixing valves; the central angle is proportional to the distance between the mixing valves (mixing valve width: 200 μm). (b) Width variation of mixing valves; distance between the mixing valves is equivalent to that of the mixer whose central angle between the mixing valves and mixing valve width is 45° and 200 μm. (c) Shape variation of mixing loop; distance between the mixing valves is equivalent to that of the circular mixer whose central angle between the mixing valves is 30° (mixing valve width: 200 μm).

on the mixing performance, we varied the distance between the mixing valves, the mixing valve width, and the mixing loop shape. In mixer chips A and B, as shown in Fig. 3(a), we varied the distance between the mixing valves by changing the central angle between the mixing valves in the circular mixing loop from 10° to 90°. Fig. 3(b) shows that the mixing valve width was varied from 100 μm to 300 μm in mixer chip C with a constant distance between the mixing valves. In addition to circular loops, triangular and rectangular loops were used in mixer chip D, as shown in Figure 3(c). Since the triangular loop has three 120° bends and the rectangular loop has four 90° bends, the effect of the bend on mixing performance can be investigated. The typical dimensions of the flow channels are 100 μm in width and 10 μm in height for all mixer chips. The height of the control channels is 10 μm. The width of the control channels is 50 μm except for the valve area. For shutoff valves and mixing valves, the width is typically 200 μm and the mixing valve width is varied in mixer chip C.

We fabricated the mixer chips by the multilayer soft lithography technique.[7] Mask designs were prepared with AutoCAD software (AutoDesk, Inc.) and printed on a transparent film at 20,000 dpi (CAD/Art Services, Inc., OR, USA). By using the photoresist-based photolithographic techniques, we fabricated molds for the two layers. At first, the positive photoresist (AZ P4620) was spin-coated onto a 4 in. silicon wafer. This was followed by mask exposure and development. For reliable opening and closing of valves, the cross-sectional shape of flow channels was rounded by heating the mold at 130°C for 2 min. The top fluidic layer of the chip was made by pouring uncured polydimethylsiloxane (PDMS; GE RTV615; elastomer:crosslinker = 10:1) onto the fluidic layer mold to achieve a thickness of 5 mm. The bottom control layer of the chip was made by spin-coating uncured PDMS (elastomer:crosslinker = 20:1) onto the control layer mold at 2800 rpm for 1 min. The resultant thickness of the control layer was 30.9 ± 2 μm. The layers were cured for 1 h (fluidic layer) and 45 min (control layer) at 80°C. The fluidic layer was peeled off from the mold and holes for input/output ports to flow channels were punched with a 19-gauge punch (Syneo Co., Angleton, TX, USA). The fluidic layer was aligned over the control layer and the aligned layers were bonded by baking

at 80°C for 45 min. The bonded layers were peeled off from the control layer mold and holes for input ports to control channels were punched. Finally, the PDMS chip was covered by a pre-cleaned glass slide (Fisher Science Education PK72) and kept in an oven at 80°C for 18 h to advance adhesion. Fig. 4 shows the fabricated mixer chip and the experimental setup. We mounted the mixer chip on an optical stereomicroscope (Zeiss Stemi 2000-C) and microscope images were captured by using a digital microscope camera (Motic Moticam 1000). We processed all the captured images by using ImageJ software (http://rsb.info.nih.gov/ij/) to obtain the average gray value for the mixer area. We operated the mixer chip by a customized pneumatic control system. Since PDMS is permeable to gases, we filled the tubing connecting the pressure source to the shutoff valves with water to avoid bubble formation inside the flow channels. However, we did not fill the tubing connecting the pressure source with the mixing valves with
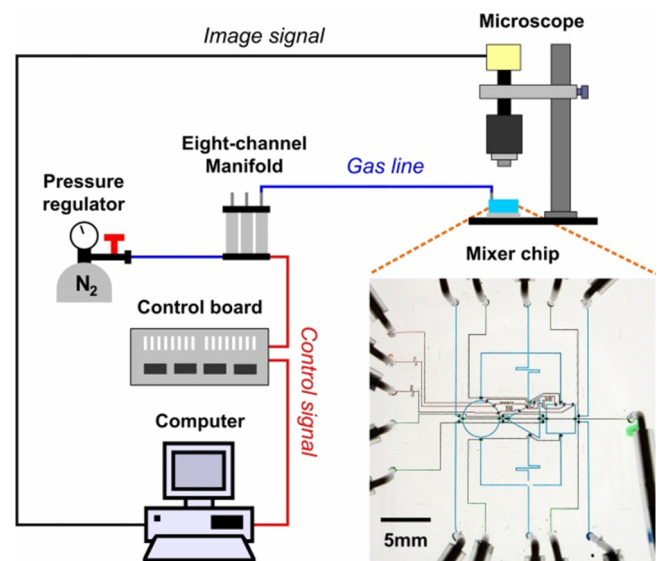

FIG. 4. Experimental setup and fabricated mixer chip (chip D); all channels of the mixer chip are filled with food dyes (flow channels: blue; control channels connected to shutoff valves: green; control channels connected to mixing valves: red) to show the planar configuration of the fabricated mixer chip.
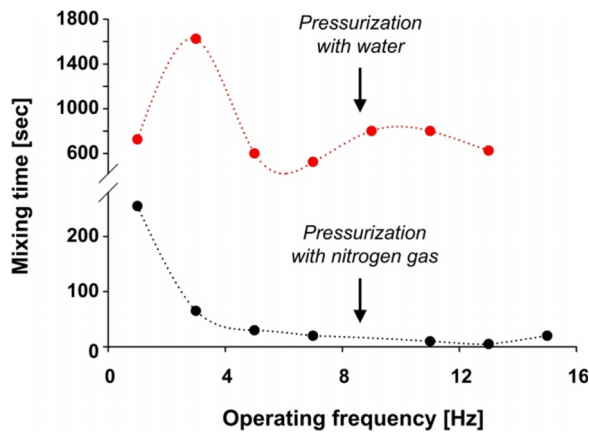
FIG. 5. Effect of pressurizing mixing valves on mixing performance; when compared with water (filled circles) which is used to pressurize the mixing valves, nitrogen gas (hollow circles) reduces the mixing time (loop shape: circle; angle between mixing valves: 30°; mixing valve width: 200 μm).

water because water-filled tubing is not highly sensitive to the applied gas pressure (Fig. 5). We used compressed nitrogen gas to pressurize the control channels. Since the viscosity of water is about one hundred times larger than that of nitrogen gas,[18] the water located between the pressure source and the mixing valves can serve as a damper for the pressure stimulation. Consequently, when the tubing connecting the pressure source with the mixing valves is filled with water, the mixing performance is decreased, as shown in Fig. 5. In addition, we calculated and found that gas permeation into the mixing loop was negligible during the experiment. The volume of gas permeation through the PDMS membrane can be calculated as follows:

$$V = \frac{P \Delta p A t}{L}, \tag{1}$$

where V, P, Δp, A, t, and L represent the volume of gas permeation, the permeability, the pressure drop across the PDMS membrane, the membrane area, the time duration for the pressure application, and the membrane thickness, respectively. For the tested cases, P, Δp, A, t, and L are 1.838 $\times 10^{-15}$ m^2/s Pa,[19] 15 psi, 0.04 mm^2, 1/78 s, and 20.9 μm. Using Equation (1), we found that the volume of gas permeation was 4.663 pl, which is less than 0.05% of the mixing loop volume. Therefore, in the present study, we maximized the mixing performance by directly pressurizing the mixing valves with nitrogen gas without concern for gas permeation. To introduce liquid food color (ESCO Foods, Inc.) into the flow channels quickly (within 5 s), we applied a pressure of 5 psi to the backside of the dyes. The pneumatic control setup consisted of three sets of eight-channel manifolds (Fluidigm Corporation) and a BOB3 control board (Fluidigm Corporation). A digital I/O card (National Instruments PCI-6533) mounted in the computer digitally controlled the switching of each channel of manifolds through the BOB3 control board. We used a custom-built LabVIEW (National Instruments) program for automatic control of the individual valves. The three mixing valves were pressurized to generate fluid flow in an isolated mixing loop with the pumping sequence of 1/2 duty cycle, 001, 011, 010, 110, 100, 101,

where 0 and 1 indicate "opened valve" and "closed valve," respectively.[11] Experiments were performed three times for each chip. From the uncertainty analysis, the uncertainty was found to be 5.0% for the 95% confidence level.

III. RESULTS AND DISCUSSION

We mixed two food dyes with viscosities that were almost equivalent to that of water (0.001 Pa·s at 20°C)[18] in the peristaltic micromixers to visualize the mixing phenomena and, using the data obtained from the photographic images, quantified the mixing performance of each mixer. Fig. 6 shows the images of the mixing phenomena that occur inside the micromixer. When the mixing valves are not operating, mixing is dominated by molecular diffusion and shows little progress even after several minutes, as shown in Fig. 6(a). However, when the mixing valves are operating, the interface between the dyes is stretched very quickly. Consequently, mixing is completed within 4 s, as shown in Fig. 6(b). To quantify the degree of mixing, we tracked the gray value change in the mixing area. Fig. 6(c) presents the change of the average gray value of the mixer area for the mixing shown in Fig. 6(b). Fig. 6(c) shows that the average gray value decreased as the degree of mixing increased. When the mixing is completed, the gray value reaches a constant value. Standard deviation of gray values for an analyzed area has been used to determine the degree of mixing.[20] However, because the average gray value changes with time as shown in Fig. 6(c), tracking the average gray value is a simpler way for quantification of the degree of mixing in the present study. To quantify the degree of mixing based on the average gray value, we define a mixing index as follows:

$$I_M \equiv \frac{G_i - G}{G_i - G_f}, \tag{2}$$

where I_M, G_i, G, and G_f represent the mixing index, the average gray values for the initial state, the given time, and the final state, respectively. Fig. 6(d) shows the mixing index change for the mixing phenomenon shown in Fig. 6(b). The mixing index is initially zero and increases as the mixing progresses. Finally, when the mixing is completed, the mixing index reaches a value of one. If the mixing time is defined as the time required for the mixing index to reach a value of 0.95, the mixing time for the case shown in Fig. 6(b) is 3.6 s. This is consistent with the estimates derived from the captured images.

The thickness of the membrane between the control channel and the flow channel was 20.9 ± 2 μm. For reliable activation of the membrane, we applied a pressure of 15 psi to the control channels. Under these conditions, we tested each mixer at various operating frequencies in order to find an optimum value. Fig. 7 shows the effect of the operating frequency on the mixing performance. Fig. 7 shows that an operating frequency of 13 Hz is the best to maximize the mixing performance. When the operating frequency is lower than cutoff frequency of the mixing valve connected to the pneumatic control setup, as the frequency increases, liquid under the mixing valve is pushed more frequently, increasing the flow rate. However, when the operating frequency exceeds the cutoff frequency, the mixing valve would fail to follow the
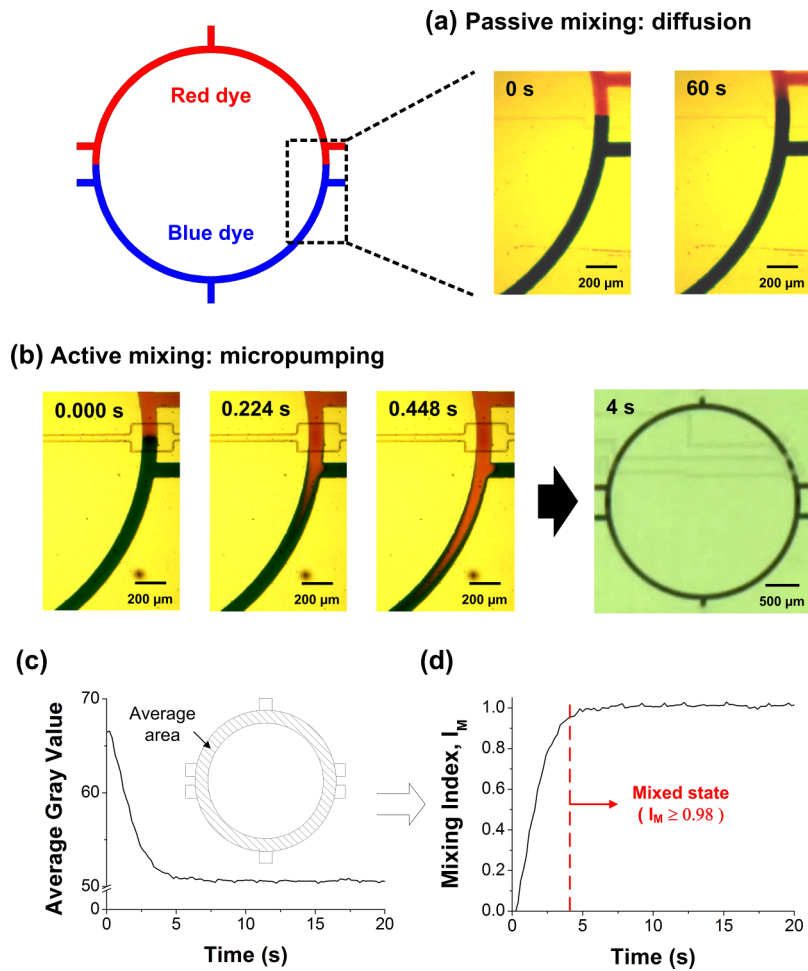
FIG. 6. Mixing phenomena in a mixer chip. (a) Mixing by molecular diffusion; boundary layer thickness increases to about 200 μm in 1 min. (b) Active mixing by mixing valve operation; mixing is completed within 4 s. (c) Quantification of the degree of mixing using the average gray value for the mixer area (hatched region); the average gray value decreases to a steady state value as the mixing progresses. (d) Mixing index using the average gray value; the mixing index increases from 0 to 1 as the mixing progresses (loop shape: circle; angle between mixing valves: 10°; mixing valve width: 200 μm; operating pressure: 15 psi; operating frequency: 13 Hz).

operating signal and incomplete closing of the valve could reduce the flow rate.[21] Figure 7 indicates that the cutoff frequency for the experimental setup in the present work must be about 13 Hz. Hence, the operating frequency was set to 13 Hz in the experimental parametric study. Under the operating conditions, we tested a mixer chip up to 12 h to check the durability and verified that none of mixing valves showed any sign of wear or fatigue.

Figs. 8(a) and 8(b) show the effect of the distance between the mixing valves on the mixing performance. The smaller the distance (central angle) between the mixing valves, the faster the mixing as shown in Fig. 8(a). To make the flow unidirectional, one valve of the three should be closed while the neighboring valve is activated. In the course of unidirectional flow generation, the liquid inside the shorter flow channel between the two valves is almost stagnant. Therefore, if we place a longer stagnant liquid between the two valves, more driving forces from the activating valve are used to push the stagnant liquid without changing the effective flow. The driving force loss is decreased with decreasing
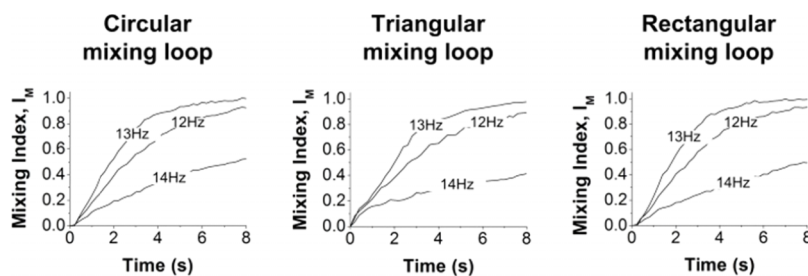

FIG. 7. Effect of operating frequency on mixing performance: the mixing index increases more rapidly when the operating frequency is 13 Hz regardless of the mixing loop shape.
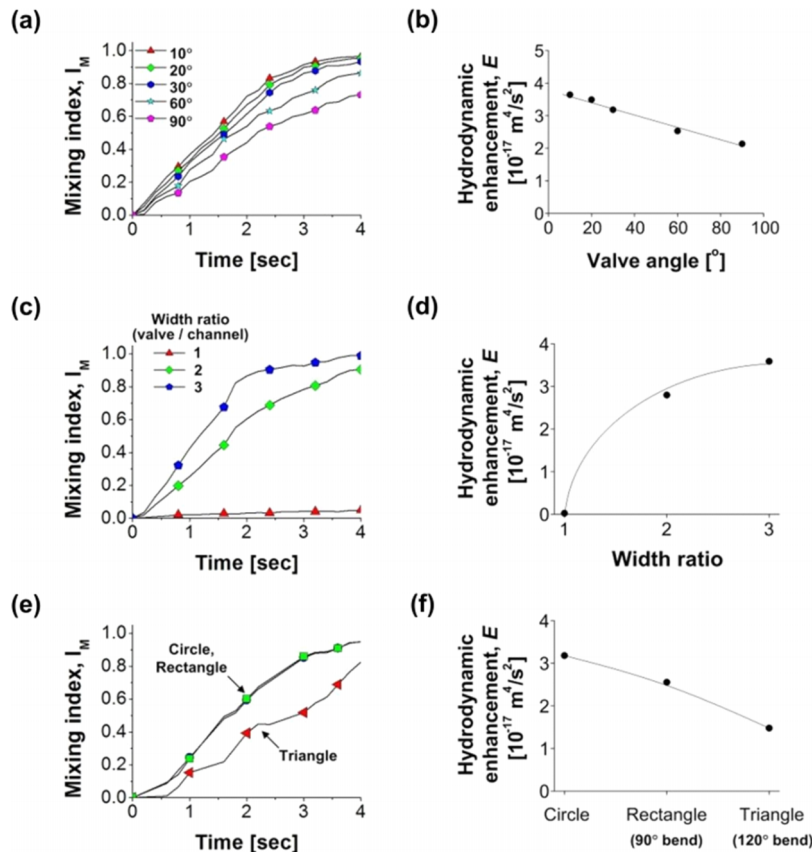
FIG. 8. Summary of parametric study. Effect of the distance between neighboring mixing valves on (a) degree of mixing and (b) hydrodynamic mixing enhancement. Effect of mixing valve width on (c) degree of mixing and (d) hydrodynamic mixing enhancement. Effect of mixing loop shape on (e) degree of mixing and (f) hydrodynamic mixing enhancement.

distance between the neighboring mixing valves. The reduced driving force loss results in effective unidirectional flow with faster stretching of the interface between the two fluids inside the microfluidic mixer. The mixing enhancement due to the interface stretching caused by the variation in the streamline velocity can be quantified by using the Taylor-Aris dispersivity. The cross-sectional shape of the tested flow channel is similar to that of single-etched isotropic channels. Hence, the Taylor-Aris dispersivity, the effective diffusivity, can be determined as follows:[22]

$$\frac{K}{D} = 1 + 0.037 Pe_H^2 = 1 + 0.037 \left(\frac{UH}{D}\right)^2 = \frac{1}{D^2}\left(D^2 + E\right),$$

(3)

where K, D, Pe_H, U, H, and E represent the Taylor-Aris dispersivity, the molecular diffusion coefficient, the Peclet number, the average fluid velocity, the flow channel height, and the degree of hydrodynamic mixing enhancement, respectively. From the captured images on the movement of the interface between fluids as shown in Fig. 6(b), we obtained the average fluid velocity and calculated the degree of hydrodynamic enhancement for each mixer. Fig. 8(b) quantitatively shows that the degree of hydrodynamic mixing enhancement resulted from the interface stretching increases with decreasing distance between mixing valves. This indicates that the distance between the valves should be as short as possible to make an effective mixer. When the central angle is 10°, the distance between the mixing valves is about 76 μm.

Considering the current state of microfabrication technology, there is still more room to enhance mixing performance. In addition to increasing the performance, decreasing the distance between the mixing valves can lead to a more efficient usage of space. This is very important for highly integrated microfluidic systems.

Figs. 8(c) and 8(d) show the effect of the mixing valve width on the mixing phenomena. We normalized the valve width with the flow channel width. As the mixing valve width is increased, the fluid volume pushed out by the movement of the valve membrane is increased. Fig. 8(d) shows that, as the valve width increases, the degree of hydrodynamic enhancement is increased due to the increased flow rate through the mixing loop. This results in faster mixing as shown in Fig. 8(c). When the ratio of the mixing valve width to the flow channel width is increased from 1 to 2, the mixing performance is significantly enhanced. However, the mixing performance enhancement is dramatically decreased as the width ratio is increased. Since the design flexibility is decreased as the footprint of the valve is increased for a given space, there would not be any merit in increasing the width ratio to a value greater than 3.

Figs. 8(e) and 8(f) show the effect of the mixing loop shape on the mixing of dyes. The rectangular mixer is almost equivalent to the circular mixer in mixing performance; however, the performance of the triangular mixer is not as good as that of the others as shown in Fig. 8(e). When there is a bend in the flow channel, there are two conflicting parameters

TABLE I. Mixing time for peristaltic micromixers.

Shape	Angle (deg)	Width (μm)	Bending	Reynolds number[a]	Mixing time (s)
	10	200	×	0.031	3.6
	20	200	×	0.030	3.9
	30	200	×	0.029	4.5
		100	×	0	>180
Circle	45[b]	200	×	0.027	5.2
		300	×	0.031	3.4
	60	200	×	0.026	5.4
	90	200	×	0.024	7.4
Triangle	30[c]	200	○	0.020	6.8
Rectangle	30[c]	200	○	0.026	4.2

[a]UH/ν (ν: Fluid kinematic viscosity).
[b]Distance between the mixing valves is equivalent to that of the mixer whose central angle between the mixing valves and mixing valve width is 45° and 200 μm.
[c]Distance between the mixing valves is equivalent to that of the circular mixer whose central angle between the mixing valves is 30°.

influencing mixing performance. The bend in the flow channel acts as an additional resistance for fluid flow and this reduces the flow rate generated by the sequential motion of the mixing valves. Fig. 8(f) shows that, as the bend angle increases, the degree of hydrodynamic enhancement is decreased due to the reduced flow rate. On the other hand, it was numerically and experimentally verified that secondary flows induced by bends in the flow channel can stir fluids, enhance mixing, and under certain conditions induce chaotic advection flow.[23,24]

Since the circular mixer, which does not have any bends in the flow channel, and the rectangular mixer have almost the same performance, we can infer that the pumping performance reduction due to the increased flow resistance and the mixing enhancement due to the secondary flows cancel each other for the rectangular mixer. However, for the triangular mixer, the effect of the reduced pumping performance is dominant and this results in worse mixing performance in comparison with other shapes. For the same mixing loop length, the footprint of the rectangular mixer is just 78.5% of that of the circular mixer. In addition to that, when multiple mixing loops are placed on a specified area, the circular shape requires more space around the mixing loop when compared with that required with the rectangular-shaped mixer. Since the rectangular shape is more advantageous than the circular shape for very large scale integration, we conclude that the rectangular-shaped mixer is the best choice for highly integrated microfluidic platforms.

All of experimental results illustrating the effects of the mixer geometry on the mixing time are summarized in Table I. Except for the mixer with a valve width equal to the flow channel width, as shown in Table I, we found that the two dyes were mixed within 10 s. It is worth noting that, when the triangle or rectangle mixer having bends in the flow channel was used, the mixing time was reduced for the same Reynolds number. However, for the same pumping setup, the Reynolds number for the triangle mixer was just 69% of that for the circular mixer with the same spacing between the mixing valves due to the bend as discussed above and the decrease in the hydrodynamic mixing enhancement increased the mixing time to 150% of that for the circular mixer. On the other hand,

for the rectangle mixer, the flow velocity reduction was less than that for the triangle mixer and the mixing enhancement due to the secondary flows dramatically decreased the mixing time to even shorter than that for the circular mixer. From the results of the experimental parametric study, we derived design guidelines for the peristaltic micromixer for highly integrated microfluidic platforms as follows:

1. The neighboring mixing valves should be as close as possible.
2. The mixing performance is increased as the mixing valve width is increased, but when both the mixing performance and the design flexibility are considered, a value of 3 is sufficient for the ratio of the mixing valve width to the flow channel width.
3. Considering both the mixing performance and the space utilization, the rectangular mixer is best for the applications of highly integrated microfluidic platforms.

IV. CONCLUSIONS

We have investigated the effects of the geometry of peristaltic micromixers on the fluidic mixing efficiency. For the parametric study, we designed and fabricated ten different mixers, varying the distance between the mixing valves, the mixing valve width, and the mixing loop shape. We mixed two food dyes in each mixer to visualize the mixing phenomena and quantified the mixing performance by analyzing the images of the mixer area. From the experimental parametric study, we have concluded three design guidelines for geometric optimization of the micromixer. First, the smaller the distance between the mixing valves, the faster the mixing. Second, a value of 3 is sufficient for the ratio of the mixing valve width to the flow channel width when both the mixing performance and the design flexibility are considered. Third, the rectangular-shaped micromixer is equal to or better than the ring-shaped microfluidic loop in terms of its mixing efficiency. The guidelines derived in the present work would greatly improve the layout of the high-throughput

integrated microfluidic systems and the overall performance by maximizing the mixing performance of the unit mixer.

[1]J. W. Hong, T. Fujii, M. Seki, T. Yamamoto, and I. Endo, Electrophoresis **22**, 328–333 (2001).

[2]M. Hamon and J. W. Hong, Mol. Cells **36**, 485–506 (2013).

[3]S. Shin, Y. J. Yoo, and J. W. Hong, J. Nanosci. Nanotechnol. **15**, 7876–7880 (2015).

[4]C. Zhang, D. Xing, and Y. Li, Biotechnol. Adv. **25**, 483–514 (2007).

[5]E. Livak-Dahl, I. Sinn, and M. Burns, Annu. Rev. Chem. Biomol. Eng. **2**, 325–353 (2011).

[6]P. N. Nge, C. I. Rogers, and A. T. Woolley, Chem. Rev. **113**, 2550–2583 (2013).

[7]M. A. Unger, H.-P. Chou, T. Thorsen, A. Scherer, and S. R. Quake, Science **288**, 113–116 (2000).

[8]S. Haeberle and R. Zengerle, Lab Chip **7**, 1094–1110 (2007).

[9]V. Studer, G. Hang, A. Pandolfi, M. Ortiz, W. F. Anderson, and S. R. Quake, J. Appl. Phys. **95**, 393–398 (2004).

[10]P. Fordyce, C. Diaz-Botia, J. DeRisi, and R. Gomez-Sjoberg, Lab Chip **12**, 4287–4295 (2012).

[11]H.-P. Chou, M. A. Unger, and S. R. Quake, Biomed. Microdevices **3**, 323–330 (2001).

[12]J. W. Hong, V. Studer, G. Hang, W. F. Anderson, and S. R. Quake, Nat. Biotechnol. **22**, 435–439 (2004).

[13]D. Kim, W. S. Lee, S. Shin, H. S. Rho, J. Dai, J. Y. Yun, and J. W. Hong, Sci. Adv. Mater. **6**, 2428–2434 (2014).

[14]S. Jambovane, E. C. Duin, S.-K. Kim, and J. W. Hong, Anal. Chem. **81**, 3239–3245 (2009).

[15]S. H. Lee, H.-W. Rhee, D. van Noort, H. J. Lee, H. H. Park, I.-S. Shin, J.-I. Hong, and T. H. Park, Biosens. Bioelectron. **57**, 1–9 (2014).

[16]J. Wang, G. Sui, V. P. Mocharla, R. J. Lin, M. E. Phelps, H. C. Kolb, and H. R. Tseng, Angew. Chem. **118**, 5402–5407 (2006).

[17]J.-C. Galas, A.-M. Haghiri-Gosnet, and A. Estévez-Torres, Lab Chip **13**, 415–423 (2013).

[18]R. W. Fox, A. T. McDonald, and P. J. Pritchard, *Introduction to Fluid Mechanics* (John Wiley & Sons, New York, 1985).

[19]M. A. Eddings and B. K. Gale, J. Micromech. Microeng. **16**, 2396 (2006).

[20]S. W. Lee, D. S. Kim, S. S. Lee, and T. H. Kwon, J. Micromech. Microeng. **16**, 1067 (2006).

[21]J. Goulpeau, D. Trouchet, A. Ajdari, and P. Tabeling, J. Appl. Phys. **98**, 044914 (2005).

[22]D. Dutta, A. Ramachandran, and D. T. Leighton, Jr., Microfluid. Nanofluid. **2**, 275–290 (2006).

[23]R. H. Liu, M. Stremler, K. V. Sharp, M. G. Olsen, J. G. Santiago, R. J. Adrian, H. Aref, and D. J. Beebe, J. Microelectromech. Syst. **9**, 190–197 (2000).

[24]M. Yi and H. H. Bau, Int. J. Heat Fluid Flow **24**, 645–656 (2003).